Eur. Phys. J. A **21**, 369–374 (2004)
DOI 10.1140/epja/i2003-10221-1

THE EUROPEAN PHYSICAL JOURNAL A

Structure of the isovector dipole resonance in neutron-rich ^{60}Ca nuclei and direct decay from pygmy resonance

T.N. Leite[a] and N. Teruya

Departamento de Física, Universidade Federal da Paraíba, CP 5008, 58051-970 João Pessoa, Pb, Brazil

Received: 22 September 2003 / Revised version: 9 February 2004 /
Published online: 7 September 2004 – © Società Italiana di Fisica / Springer-Verlag 2004
Communicated by A. Molinari

Abstract. The structure of the isovector dipole resonance in neutron-rich calcium isotope, ^{60}Ca, has been investigated by implementing a careful treatment of the differences of neutron and proton radii in the continuum random phase approximation (RPA). The calculations have taken into account the current estimates of the neutron skin. The estimates of the escape widths for direct neutron decay from the pygmy-dipole resonance (PDR) were shown rather wide, implicating a strong coupling to the continuum. The width of the giant-dipole resonance (GDR) was evaluated, bringing on a detailed discussion about its microscopic structure.

PACS. 21.10.Pc Single-particle levels and strength functions – 21.60.-n Nuclear structure models and methods – 24.30.Cz Giant resonances – 24.30.Gd Other resonances

1 Introduction

The investigation of the nuclei lying far from the β^- stability line has been an interesting and active field of the nuclear physics in the last two decades. In that region, a great number of exotic features are observed like halo/skin formation, intruders levels, new magic numbers and new kinds of collective excitation, the so-called soft and pygmy resonances. These observations have forced the review of successful theoretical tools in nuclei around the β^- stability valley [1–4].

The description of the microscopic structure of the exotic nuclei is a current topic of study and several recent works had the concern of describing the giant resonance (GR) in neutron-rich nuclei. The main questions treated are the giant-dipole resonance (GDR) behavior and the appearance of the pygmy-dipole resonance (PDR) in a nucleus with large ratio of neutron-to-proton number (N/Z). The PDR appears in medium and heavy neutron-rich nuclei, and, within the hydrodynamic sense, they are probably due to oscillation of the neutron excess against the core ($N = Z$ nucleus). The effects of the neutron excess in dipole resonances, in neutron-rich nuclei, have been extensively studied in the literature by many groups [5–13], but a complete understanding about the resonance structure has not been reached up to now. Some questions about the nature of GDR and PDR are still kept open. The preservation of the structure of the GDR as the neutron number increases, the composition of its decay modes and the need to go beyond the $1p$-$1h$ configuration to explain it [11] are some of these subjects of theoretical interest. In addition to these interesting problems on nuclear structure, the PDR in neutron-rich nuclei plays an important role in the r-process nucleosynthesis [12,13]. In this topic, the dipole strength and the widths of the PDR and GDR are important ingredients to understand the radiative neutron capture, because they are directly related with the competition between the direct and statistical mechanisms in the neutron capture process. In order to perform the studies on neutron-rich nuclei, we choose to analyze the isovector dipole resonance in the neutron-rich calcium isotope ^{60}Ca. This nucleus was not reached experimentally yet, but its microscopic structure has been investigated recently in different versions of RPA calculations [6–9], relativistic RPA (RRPA) [10] and phonon damping model (PDM) [11].

In this work we are interested in studying the role of continuum, as well as the decay width, in the pygmy- and giant-dipole resonances in the ^{60}Ca nucleus. In these extremely fragile nuclear systems, close to the neutron drip line, the neutron density extends far away from the proton density, forming the "neutron skin". Thus, to perform these continuum calculations, we have implemented a careful treatment of the differences of neutron and proton radii in a version of the continuum RPA approach of ref. [14].

In sect. 2 of this paper, we describe the theoretical approach used in the calculations. In sect. 3 we present and comment our results.

[a] e-mail: tnleite@fisica.ufpb.br

2 Theoretical approach

The continuum effects in our microscopic calculations are taken into account through a discrete particle-hole basis which accomodates the single-particle resonance widths, resulting in a diagonalization of RPA-like complex matrices of standard size [14]. The excited states are implemented in the particle-hole excitation space, and the open channels correspond to unbound particle-hole states with complex energies, of which the imaginary parts give the single-particle escape widths. We assume the nuclear Hamiltonian of the form $H = H_0 + \frac{1}{2}\sum_{i\neq j} V_{ij}$ with a mean-field part H_0 and a residual two-body force, so that $(E_\nu - H) \mid \nu\rangle = 0$ is satisfied for the nuclear excited states $\mid \nu\rangle$ with energy E_ν. Using the orthogonal and complementary projectors Q and P, the particle-hole space can be splitted into normalized bound (or unbound) particle-hole states and residual continuum states, respectively. Then, using the projection operator formalism, we have the equations

$$\left[E_\nu - H_{QQ} - H_{QP}\frac{1}{E_\nu + i\eta - H_{PP}}H_{PQ}\right]Q|\nu\rangle = H_{QP}|\,\chi^\dagger\rangle\,, \tag{1}$$

where $|\chi^\dagger\rangle$ is the appropriate scattering solution of H_{PP}:

$$[E_\nu - H_{PP}] \mid \chi^\dagger\rangle = 0. \tag{2}$$

The relevant continuum effects in P space are taken by accounting the single-particle resonance in unbound particle-hole states (taken out for the Q space), that is reached making the approach of ignoring the two-body force in P space. In this way, eq. (2) is a single-particle equation and the continuum self-energy ($H_{0QP}\frac{1}{E_\nu + i\eta - H_{0PP}}H_{0PQ}$) dresses the single-particle resonance with escape effects [15,16]. Thus, we define the complex particle-hole modes $\mid R_n\rangle$ with complex energies $\widehat{\varepsilon}_n = \varepsilon_n - \frac{1}{2}\,i\,\Gamma_n^\uparrow$ which account for continuum escape effects:

$$[\widehat{\varepsilon}_n - \hat{H}_{QQ}] \mid R_n\rangle = 0 \text{ and } [\widehat{\varepsilon}_n^* - \hat{H}_{QQ}^\dagger] \mid \widetilde{R}_n\rangle = 0\,, \tag{3}$$

$$Q \mid \nu\rangle = \sum_n \frac{\mid R_n\rangle\langle\widetilde{R}_n \mid H_{QP} \mid \chi^\dagger\rangle}{E_\nu - \widehat{\varepsilon}_n}\,, \tag{4}$$

where $\hat{H}_{QQ} = H_{QQ} + H_{QP}\frac{1}{E_\nu + i\eta - H_{PP}}H_{PQ}$ and the complex modes satisfy the orthonormalization relation: $\langle\widetilde{R}_{n'} \mid R_n\rangle = \delta_{nn'}$. The matrix element in eq. (4) is an escape amplitude related to the imaginary part of $\widehat{\varepsilon}_n$. The strength function $S_F(E) = \sum_n \frac{\Gamma_n^\uparrow}{2\pi}\frac{|\langle\widetilde{R}_n|\hat{F}_\lambda|0\rangle|^2}{(E-\varepsilon_n)^2 + (\Gamma_n^\uparrow/2)^2}$ is calculated by making the approach that the excited states $\mid \nu\rangle$ can be well described by the $Q \mid \nu\rangle$ component. In the particle-hole matrix element calculation of the 1-body operator $\widehat{F}_\lambda$ of the strength function $S_F(E)$, we have assumed the form

$$\widehat{F}_{JM} = e_k r^J Y_{JM}\,, \tag{5}$$

where e_k is the nucleon effective charge. For the isovector dipole transition, we have $e_{\nu(\pi)} = -\frac{eZ}{A}$ ($\frac{eN}{A}$).

Table 1. The Woods-Saxon central and spin-orbit parameters used in the calculations.

$V_R(r) = V_{0R}f(r)$; $V_{ls}(r) = V_{0ls}\left(\frac{\hbar}{m_\pi c}\right)^2\frac{1}{r}f'(r)\mathbf{l}\cdot\mathbf{s}$ $f(r) = \frac{1}{1+e^{(r-R)/a}}$; $a = 0.60\,\text{fm}$; $V_{0ls} = 6.54\,\text{MeV}$		
Particle	V_{0R} (MeV)	R (fm)
ν	54.5	4.30
π	65.5	4.62

The complex particle-hole modes $\mid R_n\rangle$ in eq. (3) are solved by a diagonalization of the discrete RPA equations in Q space:

$$\begin{pmatrix} A & B \\ -B & -A \end{pmatrix}\begin{pmatrix} X^n \\ Y^n \end{pmatrix} = \widehat{\varepsilon}_n \begin{pmatrix} X^n \\ Y^n \end{pmatrix}\,, \tag{6}$$

where

$$A_{php'h'} = (\widehat{\varepsilon}_p - \varepsilon_h)\delta_{pp'}\delta_{hh'} + V_{ph'hp'}\ ;\ B_{php'h'} = V_{pp'hh'} \tag{7}$$

and $\widehat{\varepsilon}_p$ ($\widehat{\varepsilon}_p = \varepsilon_p - \frac{1}{2}\,i\,\Gamma_p$) are the complex energies of the single-particle resonances [15,16]. Diagonalizing the complex equation (6), we have the complex eigenvectors $\mid R_n\rangle$ (given by complex X_{ph}^n and Y_{ph}^n amplitudes) and complex eigenvalues $\widehat{\varepsilon}_n$. Thus, in this discrete particle-hole subspace, the escape width is associated with the contribution of all allowed unbound particles coupled to their respective single holes. The partial escape width for each single hole can be approximated for $\Gamma_h^{n\uparrow} \simeq \sum_p \left|X_{ph}^n\right|^2 \Gamma_p$, and this gives a good estimate of the escape width composition for the population of several single holes in the residual nucleus.

The discrete single-particle energies are evaluated by solving the Schrödinger equation with Woods-Saxon potential, including the centrifugal and Coulomb (as a uniformly charged sphere) terms. The positive single-particle energy and its respective width are calculated in a projection technique to the continuum discretization approach [15,16]. The potential parameters of ^{60}Ca were adjusted following the systematics of the nucleon binding energy for this nucleus, because there is no experimental data available for this nucleus. ^{60}Ca is expected to have a small, but positive, neutron energy separation and a large proton energy separation ($S_n \approx 3.5$ MeV and $S_p \approx 25$ MeV). As a consequence, the single-particle potential of the proton should be deeper than the neutron one. Moreover, since ^{60}Ca is already close to the neutron drip line, the next nucleus with full neutron subshell, ^{70}Ca, should be not stable against neutron emission. In table 1, the potential parameters are displayed. The single-particle energies calculated with these parameters are very similar to those resulting from the self-consistent Hartree-Fock (HF) calculation with SIII Skyrme interaction [17,18], except for the first neutron excited state, namely the $1g_{9/2}$ level, which was evaluated to be unbound ($\varepsilon_{1g_{9/2}} \simeq 0.9$ MeV), although, in other calculations, it has been foreseen in a negative energy close to the border of the potential well. However, these differences do not affect

Table 2. Parameters of the harmonic-oscillator radial wave functions and residual interaction.

^{60}Ca						
$\sqrt{\langle r^2\rangle_\nu}$ (fm)	R_ν (fm)	a_ν (fm)	$\sqrt{\langle r^2\rangle_\pi}$ (fm)	R_π (fm)	a_π (fm)	$\sqrt{\langle r^2\rangle}$ (fm)
4.03	4.34	0.60	3.62	3.68	0.60	3.90
b_ν (fm)			b_π (fm)			
2.09			2.11			
C_0 (MeV fm^3)	$f^{\rm in}$	$f^{\rm ex}$	$f'^{\rm in}$	$f'^{\rm ex}$	g	g'
300.0	−0.002	−2.1	0.76	2.3	0.51	0.70

our results for the calculated escape widths, because this is a very narrow resonance ($\Gamma_{1g_{9/2}} < 1.0$ keV).

The RPA calculation is done by utilizing the Landau-Migdal residual interaction:

$$V_{ph}(\overrightarrow{r_1},\overrightarrow{r_2}) = C_0[f(r_1) + f'(r_1)\overrightarrow{\tau_1}\cdot\overrightarrow{\tau_2} + \\ +\overrightarrow{\sigma_1}\cdot\overrightarrow{\sigma_2}\,(g(r_1) + g'(r_1)\overrightarrow{\tau_1}\cdot\overrightarrow{\tau_2})]\delta(\overrightarrow{r_1}-\overrightarrow{r_2})\,, \qquad (8)$$

where f, f', g and g' are dimensionless and density-dependent parameters:

$$F(r) = F^{\rm ex} + (F^{\rm in} - F^{\rm ex})\xi(r)\,. \qquad (9)$$

The set of the interaction parameters is similar to that used in refs. [19,20], and it was adjusted to eliminate the spurious state 1^- (see table 2) and to reproduce the first 3^- excited state around 2.0 MeV.

We have considered a two-parameter Fermi distribution to represent the density dependence $\xi(r)$ in eq. (9). In previous calculations, we had assumed

$$\xi(r) = \frac{1}{1+e^{(r-R)/a}}\,, \qquad (10)$$

where R and a are the half-density radius and diffuseness, respectively. Nevertheless, in the present context, it is more appropriate to separate this function into neutron and proton parts:

$$\xi(r) = \frac{N}{A}\xi_\nu(r) + \frac{Z}{A}\xi_\pi(r)\,, \qquad (11)$$

where each part is given by

$$\xi_k(r) = \frac{1}{1+e^{(r-R_k)/a_k}}\,. \qquad (12)$$

Here $k = \nu(\pi)$ for neutron (proton). The Fermi distribution parameters are adjusted to reproduce the neutron and proton expected root mean square radii for the nucleus considered. It has been observed that the neutron root mean square radius ($\sqrt{\langle r^2\rangle_\nu}$) becomes larger than the respective proton radius ($\sqrt{\langle r^2\rangle_\pi}$) as the neutron number increases, keeping constant the proton number. The difference between those radii, $\Delta r_{\nu\pi} = \sqrt{\langle r^2\rangle_\nu} - \sqrt{\langle r^2\rangle_\pi}$, gives the measurement of the "neutron skin". Some estimates of $\Delta r_{\nu\pi}$ have been extracted from experimental charged radii [21–24]. We perform the R_k and a_k adjustment using the fact that for a two-parameter Fermi distribution ($\rho_k(r) \propto \xi_k(r)$) the mean square radius is given by [25]

$$\langle r^2\rangle_k = \frac{\int_0^\infty \rho_k(r) r^4 {\rm d}r}{\int_0^\infty \rho_k(r) r^2 {\rm d}r} \approx \frac{3}{5}R_k^2 + \frac{7}{5}\pi^2 a_k^2\,. \qquad (13)$$

In our RPA calculation, we represent the radial single-particle orbits by harmonic-oscillator radial wave functions $R_i(r)$ which are characterized by a size parameter b, and we have adopted a two-parameters Fermi density dependence in the residual interaction. Since the neutron and proton densities are too different in exotic nuclei, we must pay special attention with the parameter b. Therefore, we have performed a careful choice of the parameter b to analyze the microscopic structure of this exotic nucleus. In this way, using the radial distribution of the harmonic oscillator, $\rho_k(r) = \rho_k^0 \sum_{\varepsilon_i \le \varepsilon_F} (2j_i+1)\, R_i^2(r;b_k)$, in order to calculate $\langle r^2\rangle_k$, we satisfy this requisition by assuming different size parameters for neutrons and protons,

$$b_k^2 \approx \frac{4}{(3)^{\frac{4}{3}}}\langle r^2\rangle_k (X_k)^{-\frac{1}{3}}\,, \qquad (14)$$

where $X_k = N$ (Z) for $k = \nu(\pi)$ and $\langle r^2\rangle_k$ is given by eq. (13). In table 2, we have displayed the R_k and a_k adjustment based on some recent radii estimates [26–28].

3 Discussion and conclusions

In this section, we present and discuss some results which we have obtained by using $1p$-$1h$ continuum RPA approach, as described in the previous section, for the isovector dipole electric transition for ^{60}Ca. The single-particle(hole) energy levels were taken from the $1s_{1/2}$ hole up to $1g_{7/2}$ particle orbits. In this case, the core ($N = Z = 20$) is formed by neutrons and protons filling the energy levels up to the *sd* shell and the neutrons excess occupying the pf shell above the core. The calculated strength function $S_F(E)$ is displayed in the fig. 1.

In the ^{40}Ca nucleus, the GDR is located around an energy (~ 20 MeV) above the proton ($S_p \approx 8$ MeV) and neutron ($S_n \approx 16$ MeV) separation energy [29,30]. Consequently, the proton and neutron emission competes by decay of this mode. Taking into account the neutron-rich

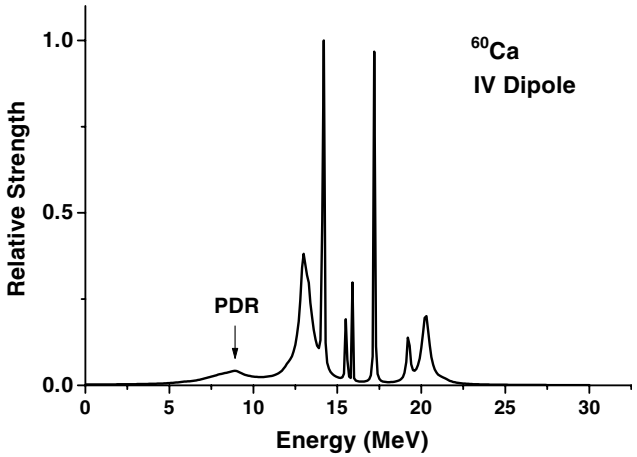

Fig. 1. The calculated strength function $S_F(E)$ by the continuum RPA approach for the $E1$ excitation in the ^{60}Ca nucleus. The wide peak at $\sim$ 8.6 MeV is in the energy interval where the PDR is expected.

nucleus (^{60}Ca), the theoretical predictions have displayed that PDR appears below the GDR as a result of neutron excess. The PDR and GDR are expected to appear below 10 MeV and 15–20 MeV [6–11], respectively. The GDR is shifted down due to the increase of the mass. However, its microscopic structure is found to be composed mainly by the single holes that belong to the most internal structure of the core, showing that they belong to the same category of excitations of the ^{40}Ca. As we have considered $S_n \approx 3.5$ MeV and $S_p \approx 25$ MeV for the ^{60}Ca nucleus, the one-neutron channel is presumed to be open in the PDR region.

According to previous RPA calculations [6–9], our calculations also predict a considerable strength in the energy region below 10 MeV, and this can be observed by the presence of the broad neutron peak in the low-lying energy in fig. 1. The broad width is due to the fact that the energy of the resonance is above the small neutron separation energy, implicating a strong coupling of the external neutrons to the continuum region. These low-lying energy states are the natural candidates for PDR because they have a dominant contribution of "neutron skin" (pf shell), in agreement with the hydrodynamic interpretation. In fig. 1 the wide peak at $\sim$ 8.6 MeV is composed by the overlap of three main peaks (see table 3) exhausting about 8% of the Energy-Weighted Sum Rule (EWSR), which is composed by transitions involving neutrons of "skin" ($2p$ and $1f \rightarrow 3s$, $2d$ and $1g$). This aspect becomes more clear when the structure of the RPA wave function of these peaks is observed. The wave functions of the states at 8.05 MeV, 8.69 MeV and 8.94 MeV are composed by the main neutron $1p$-$1h$ configurations: $\left(76\% \left|1f_{5/2}^{-1}2d_{3/2}\right\rangle_\nu + 14\% \left|2p_{1/2}^{-1}3s_{1/2}\right\rangle_\nu\right)$, $\left(93\% \left|2p_{1/2}^{-1}2d_{3/2}\right\rangle_\nu + 6\% \left|2p_{3/2}^{-1}2d_{3/2}\right\rangle_\nu\right)$ and $\left(88\% \times \left|2p_{3/2}^{-1}2d_{5/2}\right\rangle_\nu + 9\% \left|1f_{7/2}^{-1}1g_{9/2}\right\rangle_\nu\right)$, respectively, showing that each one of these peaks has a dominance of two

Table 3. The evaluated escape widths, and the estimates of the partial escape widths for each single hole, of the three main peaks that compose the PDR in $\sim$ 8.6 MeV of excitation energy (see fig. 1) exhausting about 8% of the EWSR.

$\varepsilon_n - \frac{1}{2}\, i\, \Gamma_n^{\uparrow}$ (MeV)	Single hole	$\Gamma_h^{n\uparrow}$ (MeV)
8.05–i 1.29	$(1f_{5/2})_\nu$	2.26
	$(2p_{1/2})_\nu$	0.39
	$(2p_{3/2})_\nu$	0.02
8.69–i 1.35	$(1f_{5/2})_\nu$	0.05
	$(2p_{1/2})_\nu$	2.65
	$(2p_{3/2})_\nu$	0.20
8.94–i 0.40	$(1f_{5/2})_\nu$	0.04
	$(2p_{1/2})_\nu$	0.09
	$(2p_{3/2})_\nu$	0.71

Table 4. Estimates for the mean values of the escape widths for the PDR.

$\overline{\varepsilon}_n - \frac{1}{2}\, i\, \overline{\Gamma}_n^{\uparrow}$ (MeV)	Single hole	$\overline{\Gamma}_h^{n\uparrow}$ (MeV)
8.6–i 1.3	$(1f_{5/2})_\nu$	0.7
	$(2p_{1/2})_\nu$	1.6
	$(2p_{3/2})_\nu$	0.2

$1p$-$1h$ configurations. These results are in agreement with the HF + RRPA calculation of ref. [10], where they have noticed that one-, or at most two-neutron $1p$-$1h$ configurations, determine the structure of the low-energy states for the isovector dipole resonance in ^{60}Ca, in contrast to the structure of the collective states which are characterized by a coherent superposition of many $1p$-$1h$ excitations. However, the PDR is composed by the overlap of those three main states, and the collectivity can be understood through the participation of all particle-hole components that belong to this overlap. The estimates of the partial widths $\Gamma_h^{n\uparrow}$ of the main neutrons single-holes that populate the PDR are presented in table 3. We have also evaluated an average width for the PDR, calculated as the weighted average of the widths of the peaks that compose it (see table 4), the weights being the intensities of each peak relative to the 8% of the EWSR that they exhaust. In comparision to these predictions to the PDR, we can note an apparent lack of neutron escape in the region of energy around 15 MeV, namely the GDR region, where the peaks are very narrow (see fig. 1). These peaks are constituted principally by bound $1p$-$1h$ configurations of protons and their narrow widths are due to the small neutrons amplitudes in this energy interval, reflecting an unexpected suppression of the neutron emission. This result is mainly due to the change of status of the neutrons single-particle levels, because those neutrons of the pf shell, that belonged to the configurations of the particle states in the ^{40}Ca nucleus, have become hole states in the neutron-rich nucleus, and their contributions for the GDR of the ^{60}Ca are small (they are mainly responsible for the PDR appearance). Furthermore, the composition of these narrow peaks is owed mainly to the bound $1p$-$1h$ pairs of protons.

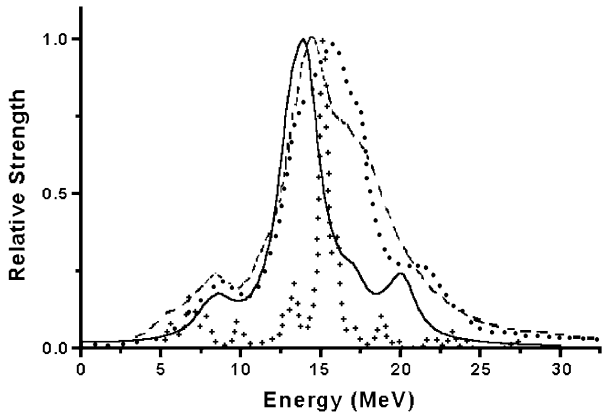

Fig. 2. Comparison among our results (solid line) with the one of other works: HF + RPA calculations by Catara *et al.* [6] (dotted line), Hamamoto *et al.* [9] (dashed line) and HF + RRPA calculations by Vretenar *et al.* [10] (crosses). Our calculation is performed by including an arbitrary constant width $\Gamma = 1.0$ MeV, instead of calculated single-particle widths used in the calculation presented in fig. 1.

This neutron lack can indicate that the GDR decay should also have more complex contributions than $1p$-$1h$ excitations. The analysis of the underlying structure of the resonance in the exotic nuclei may help us understand such disagreements because the GDR could have a more complex structure than $1p$-$1h$ configurations, which could contribute to the spreading width. To simulate these more complex structures of the GDR, we display in fig. 2 our calculation using a constant width $\Gamma = 1.0$ MeV, instead of the single-particle widths used in the calculation presented in fig. 1, and we compare the results with the ones of refs. [6,9,10]. Moreover, the two-neutron separation energy ($S_{2n} \approx 7$ MeV) is expected to be much smaller than S_p in the neutron-rich nuclei [27]. Then the two-neutron channel is presumed to be open above the PDR and below the GDR energy, and it is expected to constitute an important part of GDR decay. As our continuum RPA calculations have taken into account only $1p$-$1h$ configurations, this two-neutron emission is not considered. Therefore, the inclusion of $2p$-$2h$ configuration in the calculations would enhance the neutron emission by the GDR.

At present, it may be difficult, or else impossible, to make the experimental measures of these widths, but it could be worthwhile doing a theoretical effort for a better understanding of the microscopic structure of these exotic nuclei, that would allow us to accomplish some estimates. In ref. [13] the low-energy dipole strength, in the capture cross-section calculation, is folded by a Lorentzian curve of width $\Gamma_{\rm PDR} = \Gamma_{\rm GDR}\,(E_{\rm PDR}/E_{\rm GDR})^2$, and it is added to the GDR strength to satisfy the classical sum rule for the total $E1$ strength. We could use this relation to perform an evaluation of the $\Gamma_{\rm GDR}$. In table 4 we show the mean values of the energy (8.6 MeV) and escape width (2.6 MeV) for the PDR. The large value of the escape width could suggest that it is the main component of its total width, or $\Gamma_{\rm PDR} = 2.6$ MeV. On the other hand, our calculation gives a narrow GDR centered in 15 MeV. In spite of our calculation does not contain $2p$-$2h$ or more complex excitations, we can use these results for PDR and GDR, together the above expression [13] for the $\Gamma_{\rm PDR}$, to evaluate the width $\Gamma_{\rm GDR}$. Proceeding this way, we obtain $\Gamma_{\rm GDR} = 7.9$ MeV. This result shows that the GDR is a very wide resonance, but with a small $1p$-$1h$ escape width, and reinforces the above statement about the possible complexity of the GDR structure. The connection of these two different calculations supplies a value for the $\Gamma_{\rm GDR}$ that is close to the result obtained in the PDM calculations of ref. [11].

In short, our approach has been describing consistently the $1p$-$1h$ microscopic nature of the PDR excitation mode. The transitions in this region are composed by $1p$-$1h$ excitations involving neutrons of "skin". The broad peaks are due to the coupling to the continuum, which is extremely important in these fragile systems. Furthermore, we have exhibited an estimate about the direct escape of neutrons from PDR. Regarding the GDR, due to small escape width obtained in our calculations, the results indicate that excitations more complicated than $1p$-$1h$ should also be important for the description of its microscopic structure.

This work was supported in part by Conselho Nacional de Desenvolvimento Científico e Tecnológico (CNPq), Brazil.

References

1. I. Tanihata, R. Kanungo, C. R. Phys. **4**, 437 (2003)
2. E. Caurier, F. Nowacki, A. Poves, Nucl. Phys. A **693**, 374 (2001).
3. P.D. Cottle, K.W. Kemper, Phys. Rev. C **66**, 061301 (2002).
4. T. Hartmann, J. Enders, P. Mohr, K. Vogt, S. Volz, A. Zilges, Phys. Rev. Lett. **85**, 274 (2000).
5. J. Chambers, E. Zaremba, J.P. Adams, B. Castel, Phys. Rev. C **54**, R2671 (1994).
6. F. Catara, E.G. Lanza, M.A. Nagarajan, A. Vitturi, Nucl. Phys. A **624**, 449 (1997).
7. E.G. Lanza, Nucl. Phys. A **649**, 344c (1999).
8. P.-G. Reinhard, Nucl. Phys. A **649**, 305c (1999).
9. I. Hamamoto, H. Sagawa, X.Z. Zhang, Phys. Rev. C **57**, R1064 (1998).
10. D. Vretenar, N. Paar, P. Ring, G.A. Lalazissis, Nucl. Phys. A **692**, 496 (2001).
11. N.D. Dang, T. Suzuki, A. Arima, Phys. Rev. C **61**, 064304 (2000); N.D. Dang, V. Kim Au, T. Suzuki, A. Arima, Phys. Rev. C **63**, 044302 (2001).
12. S. Goriely, E. Khan, Nucl. Phys. A **706**, 217 (2002).
13. S. Goriely, Phys. Lett. B **436**, 10 (1998).
14. N. Teruya, A.F.R. de Toledo Piza, H. Dias, Nucl. Phys. A **556**, 157 (1993).
15. N. Teruya, A.F.R. de Toledo Piza, H. Dias, Phys. Rev. C **44**, 537 (1991).
16. T.N. Leite, N. Teruya, H. Dias, Int. J. Mod. Phys. E **11**, 469 (2002).
17. S. Im, J. Meng, Phys. Rev. C **61**, 047302 (2000).
18. I. Hamamoto, H. Sagawa, X.Z. Zhang, Phys. Rev. C **64**, 024313 (2001).

19. S. Kamerdzhiev, G. Tertychny, J. Speth, J. Wambach, Nucl. Phys. A **577**, 641 (1994).
20. S. Kamerdzhiev, J. Speth, G. Tertychny, Nucl. Phys. A **624**, 328 (1997).
21. A. Trzcińska *et al.*, Phys. Rev. Lett. **87**, 082501 (2001).
22. J. Duflo, A. P. Zuker, Phys. Rev. C **66**, 051304(R) (2002).
23. H.D. Wohlfahrt *et al.*, Phys. Rev. C **23**, 533 (1981).
24. R.H. McCamis *et al.*, Phys. Rev. C **33**, 1624 (1986).
25. L.L. Salcedo, E. Oset, M.J. Vicente-Vacas, C. Garcia-Recio, Nucl. Phys. A **484**, 557 (1988).
26. S.Q. Zhang, J. Meng, H. Toki, I. Tanihata, S.-G. Zhou, arXiv: nucl-th/0302032.
27. J. Meng *et al.*, Phys. Rev. C **65**, 041302(R) (2002).
28. Y. Sugahara, H. Toki, Nucl. Phys. A **579**, 557 (1994).
29. D. Brajnik *et al.*, Phys. Rev. C **9**, 1901 (1974).
30. H. Diesener *et al.*, Phys. Rev. Lett. **72**, 1994 (1994).